

# Current Biology

## Bidirectional Frontoparietal Oscillatory Systems Support Working Memory

### Highlights

- Brain lesions to PFC dissociate PFC and parieto-occipital systems in working memory
- The slow oscillatory substrate of executive control originates in PFC
- Parieto-occipital rhythms support working memory independent of PFC
- Frequency multiplexing supports bidirectional PFC-parieto-occipital communication

### Authors

Elizabeth L. Johnson, Callum D. Dewar, Anne-Kristin Solbakk, Tor Endestad, Torstein R. Meling, Robert T. Knight

### Correspondence

eljohnson@berkeley.edu

### In Brief

Johnson et al. show that bidirectional multiplexing between PFC delta-theta rhythms and parieto-occipital alpha-beta rhythms governs working memory. Data from patients with discrete PFC lesions reveal that the parieto-occipital rhythmic substrate provides adequate resources for working memory, challenging dominant models on the central role of PFC.



# Bidirectional Frontoparietal Oscillatory Systems Support Working Memory

Elizabeth L. Johnson,<sup>1,2,7,\*</sup> Callum D. Dewar,<sup>1</sup> Anne-Kristin Solbakk,<sup>3,4,5</sup> Tor Endestad,<sup>3</sup> Torstein R. Meling,<sup>3,4,6</sup> and Robert T. Knight<sup>1,2</sup>

<sup>1</sup>Helen Wills Neuroscience Institute, University of California, Berkeley, Berkeley, CA 94720, USA

<sup>2</sup>Department of Psychology, University of California, Berkeley, Berkeley, CA 94720, USA

<sup>3</sup>Department of Psychology, Faculty of Social Sciences, University of Oslo, Oslo 0373, Norway

<sup>4</sup>Department of Neurosurgery, Division of Clinical Neuroscience, Oslo University Hospital, Rikshospitalet, Oslo 0372, Norway

<sup>5</sup>Department of Neuropsychology, Helgeland Hospital, Mosjøen 8657, Norway

<sup>6</sup>Institute of Clinical Medicine, Faculty of Medicine, University of Oslo, Oslo 0373, Norway

<sup>7</sup>Lead Contact

\*Correspondence: [eljohnson@berkeley.edu](mailto:eljohnson@berkeley.edu)

<http://dx.doi.org/10.1016/j.cub.2017.05.046>

## SUMMARY

The ability to represent and select information in working memory provides the neurobiological infrastructure for human cognition. For 80 years, dominant views of working memory have focused on the key role of prefrontal cortex (PFC) [1–8]. However, more recent work has implicated posterior cortical regions [9–12], suggesting that PFC engagement during working memory is dependent on the degree of executive demand. We provide evidence from neurological patients with discrete PFC damage that challenges the dominant models attributing working memory to PFC-dependent systems. We show that neural oscillations, which provide a mechanism for PFC to communicate with posterior cortical regions [13], independently subserve communications both to and from PFC—uncovering parallel oscillatory mechanisms for working memory. Fourteen PFC patients and 20 healthy, age-matched controls performed a working memory task where they encoded, maintained, and actively processed information about pairs of common shapes. In controls, the electroencephalogram (EEG) exhibited oscillatory activity in the low-theta range over PFC and directional connectivity from PFC to parieto-occipital regions commensurate with executive processing demands. Concurrent alpha-beta oscillations were observed over parieto-occipital regions, with directional connectivity from parieto-occipital regions to PFC, regardless of processing demands. Accuracy, PFC low-theta activity, and PFC → parieto-occipital connectivity were attenuated in patients, revealing a PFC-independent, alpha-beta system. The PFC patients still demonstrated task proficiency, which indicates that the posterior alpha-beta system provides sufficient resources for working memory. Taken together, our findings reveal neurologically dis-

soluble PFC and parieto-occipital systems and suggest that parallel, bidirectional oscillatory systems form the basis of working memory.

## RESULTS

Examination of individuals with focal brain lesions provides evidence to draw causal links between neuroanatomy, physiology, and behavior [1, 8, 14]. We recorded 64-channel electroencephalogram (EEG) in patients with discrete lateral prefrontal cortex (PFC) lesions to investigate the influence of PFC damage on local and long-range oscillatory activities during the encoding, maintenance, and active processing of information in working memory. Fourteen unilateral PFC patients (mean ± SD: 46 ± 16 years of age; 15 ± 3 years of education; Figures 1A and S1; Table S1) and 20 age- and education-matched healthy controls completed a visuospatial working memory task. Each trial consisted of five phases: pretrial, encoding, maintenance, active processing, and response (Figure 1B). Following pretrial central fixation, two common shapes were presented sequentially in a top/bottom spatial orientation. Following the maintenance interval, the test prompt—either SAME (identity [top]), TOP/BOTTOM (spatial relation [bottom]), or FIRST/SECOND (temporal relation [bottom])—was presented to impose additional executive demands during the processing interval. This critical manipulation allowed us to examine how working memory unfolded over time, first at encoding and maintenance and then as the task required subjects to actively process information for an impending test. The encoding, maintenance, and active processing intervals were analyzed for correct-response trials, relative to the pretrial baseline.

Subjects were instructed to keep central fixation because the shapes would be presented rapidly on the left or right side of the screen at encoding [15–18], which we confirmed with eye gaze position data. This lateralized visual hemifield design capitalizes on the contralateral organization of the mammalian visual system. Stimuli presented to the right visual hemifield are initially encoded by the left hemisphere (and vice versa) and transferred via the splenium within 15 ms to engage both hemispheres, permitting both unilateral and rapid bilateral processing of visual



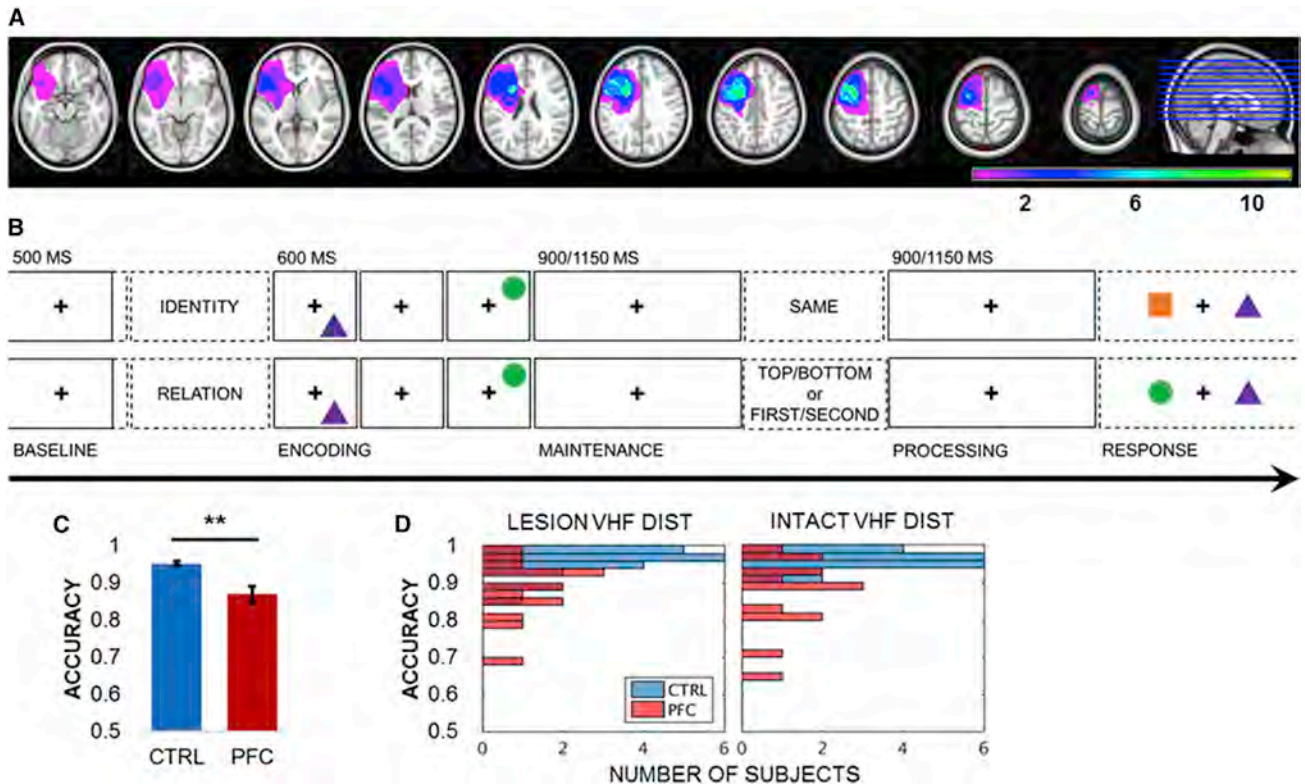


**Figure 1. PFC Patient Lesion Overlap, Working Memory Task Design, and Accuracy**

(A) Reconstruction of the extent of PFC lesion overlap for all 14 patients normalized to the left hemisphere. Color scale, number of patients with lesions at the specified site. See also Figures S1–S3 and Tables S1 and S2.

(B) Single-trial lateralized working memory task design. Following a 2-s pretrial fixation interval, subjects were cued to focus on either IDENTITY or RELATION information. Then, two common shapes were presented for 200 ms each to the left or right visual hemifield in a specific spatiotemporal configuration (i.e., top/bottom spatial and first/second temporal positions). After a 900- or 1,150-ms jittered maintenance fixation interval, the test prompt appeared, followed by an active processing fixation interval of the same length. Working memory was tested in a two-alternative forced choice test, resulting in a 0.5 chance rate. In the identity test (top), subjects indicated whether the pair was the SAME pair they just studied (correct response: no). In the spatiotemporal relation test (bottom), subjects indicated which shape fit the TOP/BOTTOM spatial or FIRST/SECOND temporal relation prompt (correct response for prompt TOP or SECOND: circle). See also Figures S2 and S3.

(C) Mean working memory task accuracy by group. Patient accuracy was attenuated relative to controls ( $p < 7 \times 10^{-5}$ ). \*\*, significant result; error bars, SEM; CTRL, controls; PFC, PFC patients; VHF, visual hemifield. See also Table S3.

(D) Single-subject histograms of working memory task accuracy by visual hemifield presentation. Accuracy did not differ by visual hemifield presentation (uncorrected  $p > 0.05$ ). DIST, distribution; CTRL, controls; PFC, PFC patients. See also Table S3.

stimuli. Recent functional magnetic resonance imaging (fMRI) data indicate that bilateral PFC is recruited for cognitively challenging tasks across the lifespan [19], suggesting that working memory recruits bilateral PFC when both hemispheres are available. Collecting EEG data in a lateralized visual hemifield design is a method to examine whether the unilaterally lesioned brain quickly compensates across hemispheres [15, 16]. Behavioral and EEG data were tested for between-groups effects depending on whether stimuli were presented to the visual hemifield contralateral to the lesioned or intact hemisphere.

We hypothesized that slow rhythms would coordinate PFC influence over parieto-occipital regions per executive demands. If working memory function is governed by PFC-dependent network control, then damage to PFC will lead to deficits in performance concomitant with altered EEG signals. Likewise, any observed effects that are not affected by damage to PFC are considered neurologically independent. First, we applied the

surface Laplacian filter to all EEG data to better isolate PFC scalp distributions and improve connectivity estimates [20–22]. We then submitted the spatial-filtered outputs to separate analyses of oscillatory metrics: event-related potentials (ERP), spectral power, and directional connectivity. Finally, we submitted the oscillatory data outputs to between-groups statistical tests using a Monte Carlo method with a conservative 95% cluster-based maximum correction for multiple comparisons [23]. All data were tested for main effects of group (i.e., patient versus control); ERP and power (i.e., within-channel) data were also tested for group  $\times$  hemisphere interactions. Hemisphere effects were modeled as indices of hemispheric asymmetry by subtracting the signal in each intact-hemisphere channel from its lesioned-hemisphere homolog (e.g.,  $F5 = F5 - F6$ ), yielding values greater than zero if lesion  $>$  intact signals and values less than zero if lesion  $<$  intact signals, and then tested for group effects. Probability values are two tailed unless otherwise specified.

## Behavior

First, we confirmed that lesion differences and other individual demographic factors, such as age and lesion etiology, did not covary with task performance in PFC patients. Patient accuracy data were submitted to a repeated-measures mixed analysis of covariance (ANCOVA) with two visual hemifield (lesion and intact) and three condition (identity, spatial relation, and temporal relation) within-subject factors, controlling for all between-subject factors (see Table S1). No significant effects were observed ( $p > 0.14$ ; Table S2), permitting the normalization of patient data into one group [24]. We then swapped right hemisphere-lesioned patient data ( $n = 7$  per hemisphere) across the midline so that lesions were normalized to the left hemisphere [15–17]. Half of the controls ( $n = 10$ ) were randomly selected for the identical swapping procedure to preclude any inter-hemispheric variation from confounding lesion-related outcomes.

Accuracy effects were tested in logit mixed-effects models [25]. Data from all subjects were submitted to a model with two group (patient and control), two visual hemifield, and three condition fixed effects and 34 subject random effects. Results revealed that PFC patients were impaired at the task relative to controls (mean  $\pm$  SD correct: controls  $0.95 \pm 0.03$  versus patients  $0.87 \pm 0.08$ ; group  $p < 7 \times 10^{-5}$ ; Figures 1C and 1D; Table S3). Nonetheless, patients performed well above chance (paired-sample  $t_{1,13} > 15.43$ ; one-tailed  $p < 5 \times 10^{-10}$ ), demonstrating that PFC does not play a unitary role in working memory. There were no differences between visual hemifield presentations or conditions (uncorrected  $p > 0.05$ ). These results permit data pooling across conditions and suggest that unilateral PFC lesions have a bilateral influence on the neural networks supporting working memory.

## Task-Induced ERPs

Analysis of ERPs demonstrated the effects of unilateral PFC lesions on a trial-wise basis dependent on visual hemifield presentation (Figure S2). ERPs were quantified between 1 and 30 Hz over the 500-ms pretrial baseline, 1,500-ms encoding-maintenance, and 900-ms active processing intervals for correct trials (see Figure 1B). Then, encoding-maintenance and processing outputs were absolute baseline corrected on the temporal mean of the pretrial baseline. Cluster-based permutation testing of ERPs revealed main effects of group early during the maintenance of stimuli that had been presented to the visual hemifield contralateral to the lesioned hemisphere. PFC patients exhibited attenuated positive-polarity ERPs in parieto-occipital channels ( $p_{\text{cluster}} = 0.03$ ) and reversed-polarity signals in lesioned-hemisphere anterior channels (F5-F7-FC5-FT7-C3-C5-T7;  $p_{\text{cluster}} = 0.002$ ). At active processing, there was a group  $\times$  hemisphere interaction ( $p_{\text{cluster}} = 0.034$ ) but no group main effect ( $p_{\text{cluster}} > 0.26$ ). Enhanced signal was detected in patients 100 ms after presentation of the test prompt in lesioned-hemisphere anterior channels (FP1-AF3-AF7-F5-F7-FC5-FT7), relative to the homologous, intact-hemisphere channels. None of these effects was observed on trials in which stimuli were presented to the intact visual hemifield ( $p_{\text{cluster}} > 0.33$ ), revealing physiological evidence that the lateralized visual hemifield presentation successfully targeted the lesioned versus intact hemisphere [15–17] and suggesting that PFC influences whole-brain networks in the service of working memory.

## Baseline Neurological Effects

Analysis of raw power during the pretrial baseline interval revealed steepening of the spectral slope over the lesioned PFC (Figure S3). Spectral power was quantified over the 500-ms pretrial baseline interval for all trials, extending from 1,450 ms after the end of the previous trial to 50 ms before the start of the current trial. The 500-ms segments were zero padded to 7,500 ms and multiplied with a Hanning taper, from which power was computed using fast Fourier transforms between 1 and 40 Hz [26]. Cluster-based permutation testing of raw power spectra revealed a group  $\times$  hemisphere interaction ( $p_{\text{cluster}} = 0.004$ ) but no main effect of group (uncorrected  $p > 0.05$ ). Enhanced power was detected between 6 and 18 Hz in lesioned-hemisphere anterior channels, relative to the homologous, intact-hemisphere channels, defining baseline effects in patients. Because these effects may partially reflect physical distortions in the EEG due to damaged tissue in the patient group, all analyses of task activity followed baseline correction.

## Task-Induced Power

Analysis of task-induced power revealed neurologically dissociable PFC and parieto-occipital oscillatory mechanisms. Spectrotemporal power was quantified for the pretrial baseline, encoding-maintenance, and active processing intervals for correct trials, and then encoding-maintenance and processing outputs were standardized on the pretrial baseline. Power was computed using a modified spectrogram approach with the same parameters as in the pretrial baseline power analysis. We computed time-frequency representations using an adaptive, frequency-dependent sliding time window of three cycles' length ( $\Delta t = 3/f$ ) and applied a Hanning taper, from which power was calculated using fast Fourier transforms [26]. Raw power outputs were Z scored against pretrial baseline distributions generated by randomly selecting baseline data samples to assess the significance of task-induced power effects per subject (i.e., statistical bootstrapping) [27].

Activity in the delta-theta (2–7 Hz) range marked the encoding-maintenance interval in anterior channels, which increased and then remained elevated through processing ( $Z > 3.29$  versus pretrial baseline;  $p < 0.001$ ; Figure S4). PFC patients did not show the same pattern of increase in anterior channels during active processing—i.e., after executive demands were imposed. Cluster-based permutation testing revealed group  $\times$  hemisphere interaction effects ( $p_{\text{cluster}} \leq 0.04$ ; Figure 2) but non-significant group main effects ( $p_{\text{cluster}} > 0.10$ ). Reduced low-theta (3–4 Hz) power was detected in anterior channels in the lesioned hemisphere, relative to the homologous channels in the intact hemisphere. The interaction effect was significant regardless of whether stimuli were initially encoded in the lesioned or intact hemisphere, revealing a bilateral PFC origin for the slow rhythmic substrate of executive control.

In contrast, increased parieto-occipital activity in the beta-gamma range (12–35 Hz) and narrowband alpha desynchronization marked visual processing during encoding, followed by widespread alpha-beta (9–24 Hz) decreases throughout maintenance ( $|Z| > 1.96$  versus pretrial baseline;  $p < 0.05$ ) and active processing ( $Z < -3.29$ ;  $p < 0.001$ ; Figure S4). These patterns did not differ by group ( $p_{\text{cluster}} > 0.52$ ), demonstrating that sustained alpha-beta suppression for working memory is

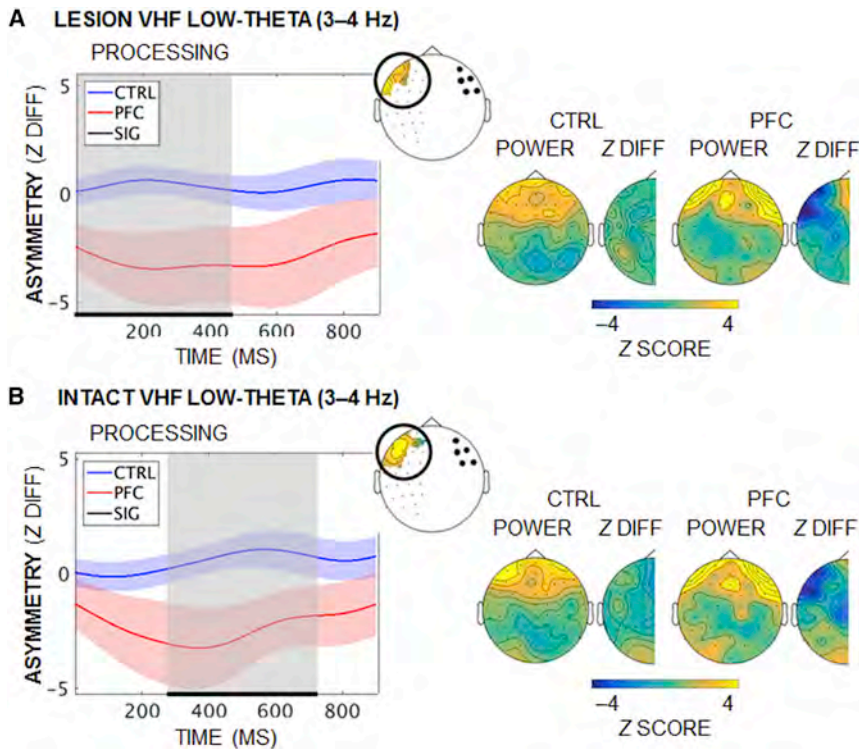


**Figure 2. Diminished Low-Theta Power in Lesioned PFC at Active Processing**

(A) Mean task-induced low-theta (3–4 Hz) hemispheric asymmetry in PFC over active processing by group when stimuli were presented to the lesioned visual hemifield. Low-theta power was diminished in patients in channels over the lesion, relative to the homologous intact-hemisphere channels (group  $\times$  hemisphere  $p_{\text{cluster}} = 0.04$ ). Left: significant effects are marked in black/gray and masked per channel on the BioSemi-64 topography (inset). Right: scalp distributions of power and hemispheric difference Z scores are presented for the period of significant effects. Whereas anterior theta power appears elevated in patients relative to controls, the contrast did not survive statistical testing (group  $p_{\text{cluster}} > 0.61$ ). Shading, SEM; Z DIFF, difference between lesioned- and intact-hemisphere Z scored power; VHF, visual hemifield. See also Figure S4.

(B) Equivalent to (A): similar low-theta power effects were observed when stimuli were presented to the intact visual hemifield (group  $\times$  hemisphere  $p_{\text{cluster}} = 0.036$ ).

independent of PFC, consistent with sources in parieto-occipital regions [28].

### Task-Induced Directional Connectivity

The temporal dynamics of directional connectivity were analyzed separately for delta-theta (2–7 Hz) and alpha-beta (9–24 Hz) oscillatory ranges using the phase slope index (PSI) [29]. PSI tracks whether the slope of the phase lag between A and B channel pairs is consistent across several adjacent frequency bins; positive PSI indicates that channel A  $\rightarrow$  B, negative PSI indicates the reverse, and zero PSI indicates either zero or an evenly balanced lead/lag relationship between channels. PSI was quantified for the pretrial baseline, encoding-maintenance, and active processing intervals for correct trials, and then raw PSI outputs were Z scored against null distributions generated by randomly shuffling the frequency bins to correct for any spurious results [22]. Finally, encoding-maintenance and processing outputs were absolute baseline corrected on the temporal mean of the pretrial baseline to assess the significance of task-induced PSI effects per subject. If PFC signals direct activity in posterior regions per executive demands, then the diminished PFC low-theta activity observed during active processing should also cause diminished PFC  $\rightarrow$  parieto-occipital PSI in patients relative to controls. Likewise, if posterior alpha-beta activity is indeed independent of PFC, then parieto-occipital  $\rightarrow$  PFC PSI should not differ by group.

PSI was visualized between the lesioned PFC region of interest, as identified in the analysis of power asymmetry (see Figure 2), and parieto-occipital channels in the same hemisphere. As shown in Figure 3 (left), analysis of delta-theta PSI revealed task-induced shifts in directionality that were selectively

impacted by PFC lesions. Parieto-occipital  $\rightarrow$  PFC PSI marked the offset of the second stimulus at encoding (baseline-corrected  $Z \leq -10$ ;  $p < 2 \times 10^{-23}$ ), suggesting the end of bottom-up information transfer along slow rhythms. Controls then exhibited a shift in directionality so that PFC drove parieto-occipital regions mid-maintenance ( $Z > 1.96$ ;  $p < 0.05$ ). PFC  $\rightarrow$  parieto-occipital PSI continued to increase in controls with executive demands such that the PFC lead peaked early during active processing ( $Z \geq 10$ ;  $p < 2 \times 10^{-23}$ ), whereas PFC patients exhibited zero directionality ( $Z < 1.96$ ;  $p > 0.05$ ). Cluster-based permutation testing of all 64-by-64 channel pairs revealed intermittent group effects during encoding and maintenance (lesioned/intact visual hemifield: 100–200/200–300 and 700–800/1,000–1,200 ms) and sustained effects during active processing (100–700/0–500 ms;  $p_{\text{cluster}} < 0.05$ ). Even when control PSI was not supra-threshold in the PFC-led direction, controls still displayed greater PFC leads than patients to widespread central-posterior sites.

We performed a post hoc graph theoretical network analysis of delta-theta PSI to assess whether diminished PFC leads in patients impacted the whole-brain connectome, as additional validation of our hypothesis. Cluster-based permutation testing of network data revealed group effects from lesioned PFC to bilateral central-posterior regions that were sustained for 200 ms early during active processing, regardless of whether stimuli were presented to the lesioned or intact visual hemifield ( $p_{\text{cluster}} \leq 0.01$ ; Figure 3, right). Taken together, these results demonstrate that PFC lesions compromise widespread parieto-occipital rhythms in the delta-theta range commensurate with executive demands, supporting our hypothesis. Because the effects were significant regardless of whether stimuli were initially encoded in the lesioned or intact hemisphere, these results further implicate a bilateral, PFC-driven frontoparietal system for executive control in the service of working memory.

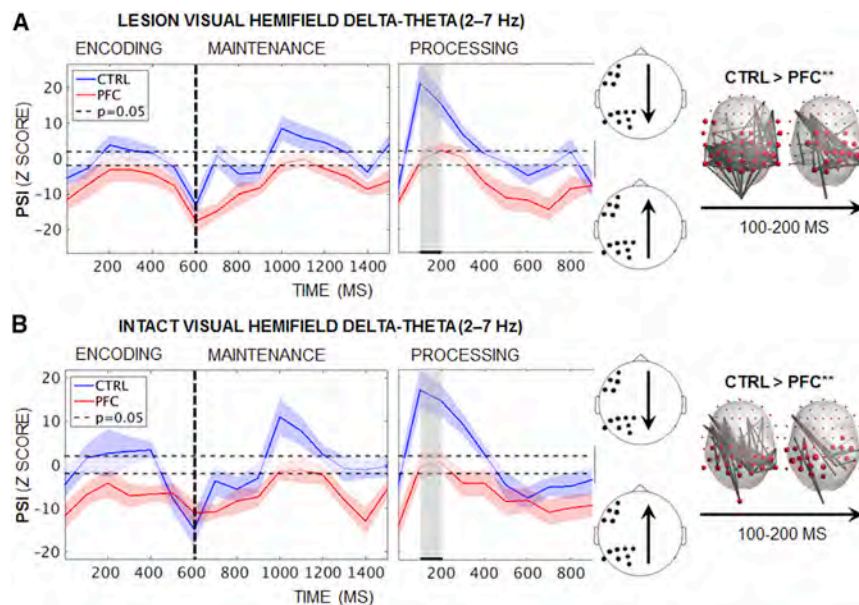


**Figure 3. Diminished PFC → Parieto-occipital Delta-Theta PSI in Patients**

(A) Mean task-induced delta-theta (2–7 Hz) PSI over encoding, maintenance, and active processing by group when stimuli were presented to the lesioned visual hemifield. Left: single-subject analyses revealed parieto-occipital → PFC PSI at the end of encoding in both groups (baseline-corrected  $Z \leq -10$ ;  $p < 2 \times 10^{-23}$ ). Controls then exhibited PFC → parieto-occipital PSI at mid-maintenance ( $Z > 1.96$ ;  $p < 0.05$ ) and early processing ( $Z \geq 10$ ;  $p < 2 \times 10^{-23}$ ), whereas patients exhibited zero directionality ( $Z < 1.96$ ;  $p > 0.05$ ). Right: group differences were maximal during active processing so that PFC damage impacted the bilateral central-posterior connectome (group  $p_{\text{cluster}} < 0.05$ ). Significant effects are masked per channel and 100-ms time point on the BioSemi-64 topography for the period of significant effects (marked in black/gray on the left). Shading, SEM; CTRL, controls; PFC, PFC patients; \*\*, significant result.

(B) Equivalent to (A): similar delta-theta PSI effects were observed when stimuli were presented to the intact visual hemifield.

In contrast, analysis of alpha-beta PSI revealed parieto-occipital → PFC PSI that was not affected by task demands or PFC damage (Figure 4). Parieto-occipital regions drove PFC throughout encoding, maintenance, and active processing, regardless of whether stimuli were presented to the lesioned or intact visual hemifield (baseline-corrected  $Z < -1.96$ ;  $p < 0.05$ ; Figures 4A and 4B). PFC lesions did not affect alpha-beta PSI at any point during encoding, maintenance, or active processing (group  $p_{\text{cluster}} > 0.05$ ). These results provide evidence for a neurologically dissociable, PFC-independent parieto-occipital origin for frontoparietal alpha-beta oscillations during working memory (Figure 4C).

## DISCUSSION

Our findings demonstrate that working memory is supported by independent frontoparietal systems, challenging dominant models that attribute working memory function to solely PFC-dependent systems [1–6]. Healthy controls exhibited task-induced low-theta activity in PFC and PFC → parieto-occipital connectivity, which shifted over time commensurate with task-processing demands. Concurrent parieto-occipital → PFC connectivity was observed in the alpha-beta range, highlighting frequency multiplexing for bidirectional frontoparietal communication. Working memory task accuracy, PFC low-theta band signals, and PFC → posterior connectivity were attenuated in patients, providing neurological evidence that the oscillatory low-theta substrate of executive control depends on PFC—and, moreover, that PFC damage impacts the PFC → parieto-occipital connectome. Nonetheless, patients still exhibited task proficiency, revealing that PFC-dependent network function is not necessary for working memory unless the task imposes additional executive demands (cf. [7, 8, 30]).

We provide the first neurological demonstration that PFC-independent alpha-beta oscillations support working memory. The recruitment of parieto-occipital regions is consistent with

theories that link working memory to the maintenance of stimuli in sensory and higher cortical areas [9–12, 31, 32]. Indeed, the widespread decreases in alpha-band power observed during delay may reflect frontoparietal control and/or recruitment of the dorsal attention network [33, 34]. The notion that such domain-general physiological signatures underpin working memory function has been proposed [35], but their mechanistic interplay with PFC remains controversial. We observed that the alpha-beta system was unaffected by PFC damage or executive demands and showed no signs of compensatory neuroplasticity. The lack of interplay with PFC is in accord with proposals that parieto-occipital alpha-beta oscillatory activity provides a core substrate for the purely mnemonic component of working memory (cf. [7, 11, 30]).

In conclusion, these findings provide evidence that independent, parallel, and bidirectional oscillatory systems form the basis of working memory, adding novel insight into the foundations of our cognitive infrastructure.

## STAR★METHODS

Detailed methods are provided in the online version of this paper and include the following:

- KEY RESOURCES TABLE
- CONTACT FOR REAGENT AND RESOURCE SHARING
- EXPERIMENTAL MODEL AND SUBJECT DETAILS
- METHOD DETAILS
  - Lesion Reconstruction
  - Behavioral Task
  - Data Acquisition
  - Data Preprocessing
  - Event-Related Potentials
  - Spectral Decomposition
  - Phase Slope Index
  - Graph Theory

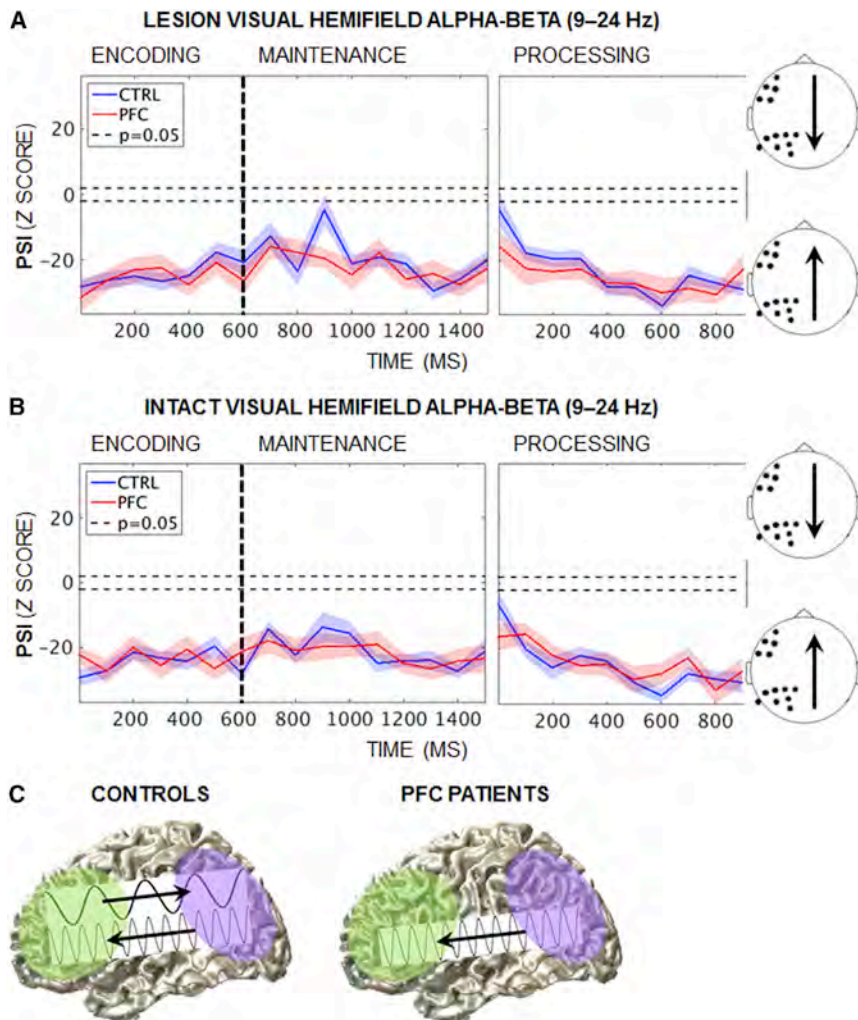


**Figure 4. Independent Parieto-occipital → PFC Alpha-Beta PSI**

(A) Mean task-induced alpha-beta (9–24 Hz) PSI at encoding, maintenance, and active processing by group when stimuli were presented to the lesioned visual hemifield. Single-subject analyses revealed independent parieto-occipital → PFC PSI (baseline-corrected  $Z < -1.96$ ;  $p < 0.05$ ) that did not differ between groups (group  $p_{\text{cluster}} > 0.05$ ). Shading, SEM; CTRL, controls; PFC, PFC patients.

(B) Equivalent to (A): similar alpha-beta PSI effects were observed when stimuli were presented to the intact visual hemifield.

(C) Schematic of neurological dissociations in frontoparietal PSI. PFC → parieto-occipital delta-theta PSI was abolished with PFC damage, whereas parieto-occipital → PFC alpha-beta PFC was unaffected, revealing a posterior alpha-beta system that is independent of PFC.

#### ● QUANTIFICATION AND STATISTICAL ANALYSES

- Behavioral Analysis
- Statistical Bootstrapping
- Cluster-Based Permutation Testing

#### ● DATA AND SOFTWARE AVAILABILITY

#### SUPPLEMENTAL INFORMATION

Supplemental Information includes four figures and three tables and can be found with this article online at <http://dx.doi.org/10.1016/j.cub.2017.05.046>.

#### AUTHOR CONTRIBUTIONS

E.L.J. designed the experiment, collected and analyzed the data, and wrote the manuscript. C.D.D. assisted with data collection and analysis, and created the lesion reconstructions. A.-K.S. and T.E. supervised data collection in Oslo, and A.-K.S. provided the Norwegian language translations. R.T.K. and T.R.M. examined the patients. R.T.K. supervised the project and edited the manuscript.

#### ACKNOWLEDGMENTS

We thank D. Scabini for coordinating all patient testing efforts in Berkeley. We also thank J. Lubell for assistance testing patients in Oslo; A. Jafarpour for

assistance writing code to process the Eyelink 1000 eyetracker data; D. Sorensen for consultation; and V. Piai, F. Foo, R.F. Helfrich, and S.M. Szczepanski for helpful discussions. This work was supported by grants from the NIH (2R37NS21135 to R.T.K.), Research Council of Norway (240389/F20 to A.-K.S., T.E., and T.R.M.), University of Oslo Internal Fund (to A.-K.S., T.E., and T.R.M.), and the Nielsen Corporation.

Received: January 24, 2017

Revised: April 12, 2017

Accepted: May 15, 2017

Published: June 8, 2017

#### REFERENCES

1. Szczepanski, S.M., and Knight, R.T. (2014). Insights into human behavior from lesions to the prefrontal cortex. *Neuron* 83, 1002–1018.
2. Miller, E.K., and Cohen, J.D. (2001). An integrative theory of prefrontal cortex function. *Annu. Rev. Neurosci.* 24, 167–202.
3. Curtis, C.E., and D'Esposito, M. (2003). Persistent activity in the prefrontal cortex during working memory. *Trends Cogn. Sci.* 7, 415–423.
4. Sreenivasan, K.K., Curtis, C.E., and D'Esposito, M. (2014). Revisiting the role of persistent neural activity during working memory. *Trends Cogn. Sci.* 18, 82–89.

5. Lara, A.H., and Wallis, J.D. (2015). The role of prefrontal cortex in working memory: a mini review. *Front. Syst. Neurosci.* *9*, 173.
6. Eriksson, J., Vogel, E.K., Lansner, A., Bergström, F., and Nyberg, L. (2015). Neurocognitive architecture of working memory. *Neuron* *88*, 33–46.
7. D'Esposito, M., and Postle, B.R. (1999). The dependence of span and delayed-response performance on prefrontal cortex. *Neuropsychologia* *37*, 1303–1315.
8. Müller, N.G., and Knight, R.T. (2006). The functional neuroanatomy of working memory: contributions of human brain lesion studies. *Neuroscience* *139*, 51–58.
9. Postle, B.R. (2016). How does the brain keep information “in mind”? *Curr. Dir. Psychol. Sci.* *25*, 151–156.
10. Ku, Y., Bodner, M., and Zhou, Y.-D. (2015). Prefrontal cortex and sensory cortices during working memory: quantity and quality. *Neurosci. Bull.* *31*, 175–182.
11. Galeano Weber, E.M., Hahn, T., Hilger, K., and Fiebach, C.J. (2017). Distributed patterns of occipito-parietal functional connectivity predict the precision of visual working memory. *Neuroimage* *146*, 404–418.
12. Bettencourt, K.C., and Xu, Y. (2016). Decoding the content of visual short-term memory under distraction in occipital and parietal areas. *Nat. Neurosci.* *19*, 150–157.
13. Helfrich, R.F., and Knight, R.T. (2016). Oscillatory dynamics of prefrontal cognitive control. *Trends Cogn. Sci.* *20*, 916–930.
14. Adolphs, R. (2016). Human lesion studies in the 21st century. *Neuron* *90*, 1151–1153.
15. Voytek, B., Soltani, M., Pickard, N., Kishiyama, M.M., and Knight, R.T. (2012). Prefrontal cortex lesions impair object-spatial integration. *PLoS ONE* *7*, e34937.
16. Voytek, B., Davis, M., Yago, E., Barceló, F., Vogel, E.K., and Knight, R.T. (2010). Dynamic neuroplasticity after human prefrontal cortex damage. *Neuron* *68*, 401–408.
17. Voytek, B., and Knight, R.T. (2010). Prefrontal cortex and basal ganglia contributions to visual working memory. *Proc. Natl. Acad. Sci. USA* *107*, 18167–18172.
18. Vendetti, M.S., Johnson, E.L., Lemos, C.J., and Bunge, S.A. (2015). Hemispheric differences in relational reasoning: novel insights based on an old technique. *Front. Hum. Neurosci.* *9*, 55.
19. Höller-Wallscheid, M.S., Thier, P., Pomper, J.K., and Lindner, A. (2017). Bilateral recruitment of prefrontal cortex in working memory is associated with task demand but not with age. *Proc. Natl. Acad. Sci. USA* *114*, E830–E839.
20. Perrin, F., Pernier, J., Bertrand, O., and Echallier, J.F. (1989). Spherical splines for scalp potential and current density mapping. *Electroencephalogr. Clin. Neurophysiol.* *72*, 184–187.
21. Kayser, J., and Tenke, C.E. (2015). Issues and considerations for using the scalp surface Laplacian in EEG/ERP research: a tutorial review. *Int. J. Psychophysiol.* *97*, 189–209.
22. Cohen, M.X. (2014). *Analyzing Neural Time Series Data: Theory and Practice* (MIT Press).
23. Maris, E., and Oostenveld, R. (2007). Nonparametric statistical testing of EEG- and MEG-data. *J. Neurosci. Methods* *164*, 177–190.
24. Cipolotti, L., Healy, C., Chan, E., Bolsover, F., Lecce, F., White, M., Spanò, B., Shallice, T., and Bozzali, M. (2015). The impact of different aetiologies on the cognitive performance of frontal patients. *Neuropsychologia* *68*, 21–30.
25. Jaeger, T.F. (2008). Categorical data analysis: away from ANOVAs (transformation or not) and towards logit mixed models. *J. Mem. Lang.* *59*, 434–446.
26. Haegens, S., Cousijn, H., Wallis, G., Harrison, P.J., and Nobre, A.C. (2014). Inter- and intra-individual variability in alpha peak frequency. *Neuroimage* *92*, 46–55.
27. Flinker, A., Korzeniewska, A., Shestuyuk, A.Y., Franaszczuk, P.J., Dronkers, N.F., Knight, R.T., and Crone, N.E. (2015). Redefining the role of Broca's area in speech. *Proc. Natl. Acad. Sci. USA* *112*, 2871–2875.
28. Hillebrand, A., Tewarie, P., van Dellen, E., Yu, M., Carbo, E.W.S., Douw, L., Gouw, A.A., van Straaten, E.C.W., and Stam, C.J. (2016). Direction of information flow in large-scale resting-state networks is frequency-dependent. *Proc. Natl. Acad. Sci. USA* *113*, 3867–3872.
29. Nolte, G., Ziehe, A., Nikulin, V.V., Schlögl, A., Krämer, N., Brismar, T., and Müller, K.-R. (2008). Robustly estimating the flow direction of information in complex physical systems. *Phys. Rev. Lett.* *100*, 234101.
30. Postle, B.R., Berger, J.S., and D'Esposito, M. (1999). Functional neuroanatomical double dissociation of mnemonic and executive control processes contributing to working memory performance. *Proc. Natl. Acad. Sci. USA* *96*, 12959–12964.
31. Ester, E.F., Sutterer, D.W., Serences, J.T., and Awh, E. (2016). Feature-selective attentional modulations in human frontoparietal cortex. *J. Neurosci.* *36*, 8188–8199.
32. Serences, J.T. (2016). Neural mechanisms of information storage in visual short-term memory. *Vision Res.* *128*, 53–67.
33. Sadaghiani, S., and Kleinschmidt, A. (2016). Brain networks and  $\alpha$ -oscillations: structural and functional foundations of cognitive control. *Trends Cogn. Sci.* *20*, 805–817.
34. Xie, Y., Feng, Z., Xu, Y., Bian, C., and Li, M. (2016). The different oscillation patterns of alpha band in the early and later stages of working memory maintenance. *Neurosci. Lett.* *633*, 220–226.
35. Postle, B.R. (2006). Working memory as an emergent property of the mind and brain. *Neuroscience* *139*, 23–38.
36. Friston, K.J., Ashburner, J., Kiebel, S.J., Nichols, T.E., and Penny, W.D. (2007). *Statistical Parametric Mapping: The Analysis of Functional Brain Images* (Academic Press).
37. Rorden, C., and Brett, M. (2000). Stereotaxic display of brain lesions. *Behav. Neurol.* *12*, 191–200.
38. Oostenveld, R., Fries, P., Maris, E., and Schoffelen, J.M. (2011). FieldTrip: open source software for advanced analysis of MEG, EEG, and invasive electrophysiological data. *Comput. Intell. Neurosci.* *2011*, 156869.
39. Delorme, A., and Makeig, S. (2004). EEGLAB: an open source toolbox for analysis of single-trial EEG dynamics including independent component analysis. *J. Neurosci. Methods* *134*, 9–21.
40. Xia, M., Wang, J., and He, Y. (2013). BrainNet Viewer: a network visualization tool for human brain connectomics. *PLoS ONE* *8*, e68910.
41. Gómez-Herrero, G. (2007). Automatic Artifact Removal (AAR) Toolbox v1.3 (Release 09.12.2007) for MATLAB (Tampere University of Technology).
42. Islam, M.K., Rastegarnia, A., and Yang, Z. (2016). Methods for artifact detection and removal from scalp EEG: a review. *Neurophysiol. Clin.* *46*, 287–305.
43. Hipp, J.F., and Siegel, M. (2013). Dissociating neuronal gamma-band activity from cranial and ocular muscle activity in EEG. *Front. Hum. Neurosci.* *7*, 338.
44. Cramer, A.O.J., van Ravenzwaaij, D., Matzke, D., Steingrover, H., Wetzels, R., Grasman, R.P.P.P., Waldorp, L.J., and Wagenmakers, E.-J. (2016). Hidden multiplicity in exploratory multiway ANOVA: prevalence and remedies. *Psychon. Bull. Rev.* *23*, 640–647.

## STAR★METHODS

### KEY RESOURCES TABLE

REAGENT or RESOURCE	SOURCE	IDENTIFIER
Deposited Data		
Raw and analyzed data	This paper	<a href="http://crcns.org">http://crcns.org</a>
Software and Algorithms		
Custom-built MATLAB code	This paper	<a href="http://crcns.org">http://crcns.org</a>
Statistical Parametric Mapping 8	[36]	<a href="http://www.fil.ion.ucl.ac.uk/spm">http://www.fil.ion.ucl.ac.uk/spm</a>
MRICron	[37]	<a href="http://www.mccauslandcenter.sc.edu/micro/mricron">http://www.mccauslandcenter.sc.edu/micro/mricron</a>
FieldTrip (release 20151205)	[38]	<a href="http://www.fieldtriptoolbox.org">http://www.fieldtriptoolbox.org</a>
EEGLAB 11.0.5.4 beta	[39]	<a href="http://sccn.ucsd.edu/eeglab">http://sccn.ucsd.edu/eeglab</a>
BrainNet Viewer 1.53	[40]	<a href="http://www.nitrc.org/projects/bnv">http://www.nitrc.org/projects/bnv</a>
Adobe Photoshop CC 2015	Adobe Systems	<a href="http://adobe.com">http://adobe.com</a>
E-Prime Professional 2.0	Psychology Software Tools	<a href="http://www.pstnet.com/eprime.cfm">http://www.pstnet.com/eprime.cfm</a>
IBM SPSS Statistics for Windows 20	IBM	<a href="http://www.ibm.com/analytics/us/en/technology/spss">http://www.ibm.com/analytics/us/en/technology/spss</a>
MATLAB 2015a	The MathWorks	<a href="http://www.mathworks.com">http://www.mathworks.com</a>

### CONTACT FOR REAGENT AND RESOURCE SHARING

Further information and requests for resources should be directed to and will be fulfilled by the Lead Contact, E.L. Johnson ([eljohanson@berkeley.edu](mailto:eljohanson@berkeley.edu)).

### EXPERIMENTAL MODEL AND SUBJECT DETAILS

We report data from 14 human adult patients with PFC lesions (mean  $\pm$  SD [range]: 46  $\pm$  16 [20–71] years of age, 15  $\pm$  3 years of education, 5 males) and 20 age- and education-matched, healthy controls (44  $\pm$  19 [19–70] years of age, 16  $\pm$  3 years of education, 11 males). Lesions were unilateral (n = 7 left + 7 right hemisphere) and focused in the inferior, middle, and/or superior frontal gyrus. All patients presented with lesions due to a single stroke or surgical resection of a low-grade tumor. Each patient was examined by a neurologist (RTK) or neurosurgeon (TRM) prior to testing, and final eligibility was determined through review of each patient's clinical MRI scan the week of testing to confirm lesion focus and stability. None of the tumor patients had evidence of tumor re-growth at the time of testing. Patients had normal/corrected-to-normal vision, estimated IQ in at least the normal range, and no other neurological or psychiatric diagnoses. For single-subject lesion reconstructions and demographic information, see [Figure S1](#) and [Table S1](#). An ANCOVA showed that individual patient factors did not covary with working memory task accuracy ( $p > 0.14$ ; [Table S2](#)), and independent-samples t tests with equal variance confirmed that the control group matched on demographics (age  $t_{1,32} < 0.36$ ,  $p > 0.72$ ; education  $t_{1,32} < 1.22$ ,  $p > 0.23$ ; variance  $F_{13,19} < 1.31$ , one-tailed  $p > 0.31$ ).

Subjects were tested at one of two sites: University of California, Berkeley (five patients with lesions due to stroke and all controls), or Oslo University Hospital (nine patients with lesions due to low-grade tumor resection). All subjects gave informed written consent in accordance with the University of California, Berkeley, Institutional Review Board or the Regional Committee for Medical Research Ethics, Region South, and in agreement with the Declaration of Helsinki.

### METHOD DETAILS

#### Lesion Reconstruction

Lesion reconstructions were created by manual delineation based on clinical MRIs obtained the week of testing ([Figures 1A and S1](#)), under the supervision of a neurologist (RTK). Fluid Attenuated Inversion Recovery (FLAIR), T1, and T2 weighted images of each patient's brain were co-registered to a T1 MNI Template using the New Unified Segmentation routine in Statistical Parametric Mapping (SPM) [36]. Lesion extents were then drawn on axial mosaics of the normalized T1 scans using MRICron [37] and Adobe Photoshop. The resulting lesion masks were converted to three-dimensional MNI space using the Mosaic to Volume routine in SPM. Lesion size was calculated using descriptive statistics in MRICron after manual delineation.

#### Behavioral Task

Working memory was tested in a single-trial, lateralized task paradigm ([Figure 1B](#)). After each 2-s pretrial fixation interval, a starting screen indicated whether the upcoming pair of stimuli would be tested for IDENTITY or spatiotemporal RELATION information. Then,

following a 100-ms central fixation interval, two common-shape stimuli were presented for 200 ms each in a specific spatiotemporal configuration (i.e., top/bottom spatial and first/second temporal positions). Stimuli were presented to the left or right of a central fixation cross to target the contralateral hemisphere [15–18]. The test prompt was presented after a 900- or 1,150-ms maintenance interval to elicit executive control mechanisms during an active processing interval of the same length. Then, two shapes were presented full-field on the horizontal axis and subjects responded in a two-alternative forced choice test, resulting in a 0.5 chance rate. In the identity test, subjects indicated whether the pair was the SAME pair they just studied; half of the pairs show two old shapes (“yes”) and half the pairs show one old shape and one new shape (“no”). In the spatial relation test, subjects indicated which shape had been on the TOP or BOTTOM, and in the temporal relation test, which shape had been presented FIRST or SECOND.

The length of the maintenance and active processing intervals was randomly jittered at 900- or 1,150-ms to preclude anticipatory mechanisms. The task was fully counterbalanced with 240 trials divided evenly into six bins (2 visual hemifield × 3 condition), chosen randomly from a pool of 270 trials with unique stimuli. The task was programmed in E-Prime Professional 2.0.

### Data Acquisition

Subjects were tested in a sound-attenuated recording room. EEG data were collected using a 64 + 8 channel BioSemi ActiveTwo amplifier with Ag-AgCl pin-type active electrodes mounted on an elastic cap according to the extended 10-20 system (BioSemi, Amsterdam, Netherlands), sampled at 1024 Hz. The horizontal electrooculogram (EOG) was recorded at both external canthi, and the vertical EOG was monitored with a right inferior eye electrode and a superior eye/frontopolar electrode. Two additional electrodes were placed on the earlobes for offline referencing. Electrode impedances were kept below 20 k $\Omega$ .

Continuous eyegaze positions were recorded to exclude any trials post hoc in which stimuli had been encoded in the ipsilateral hemifield. Berkeley eyetracking data were collected using an Eyelink 1000 optical tracker (SR Research, Ontario, Canada), sampled at 1 kHz, and Oslo eyetracking data were collected using an iView X optical tracker (SMI, Teltow, Germany), sampled at 60 Hz. Subjects' head movements were restrained using a custom wooden chin rest to minimize contamination of anterior-channel EEG traces.

An experimenter went through the behavioral task instructions and a set of six practice trials with each subject, who was permitted to repeat the practice trials by request. All subjects completed at least half of the working memory task (i.e., 60 trials per visual hemifield).

### Data Preprocessing

Preprocessing was performed blinded to group membership. EEG data were preprocessed using the FieldTrip [38] and EEGLAB [39] toolboxes for MATLAB.

### Eyegaze Position

Eyegaze position data were analyzed for both 200-ms stimulus presentation epochs. Time-resolved eyegaze positions were compared to the within-trial temporal mean position over the 100-ms central fixation interval preceding presentation of the first stimulus. Any trial in which gaze drifted from the center to include the ipsilateral visual hemifield during stimulus presentation was excluded from behavioral and EEG analyses.

### EEG Cleaning

Raw data were referenced to the mean potential of two earlobe electrodes, down-sampled to 256 Hz, filtered with 1-Hz high-pass and 70-Hz low-pass finite impulse response filters, and demeaned. Electromyography artifacts were removed automatically using the AAR external plug-in with the default 30 s sliding window [41, 42], and 60-Hz line noise harmonics (50 Hz for Oslo data) were removed using discrete Fourier transform. Then, we epoched the continuous data into trials with 1000-ms buffers, excluded any trials that had been marked based on eyegaze position, and manually inspected the data to reject any channels containing abnormal signal. Next, we used independent components analysis to remove artifacts (i.e., EOG and microsaccadic movements, auricular components, heartbeat, and residual cranial muscle activity [43]) from the remaining channels. Any channels that had been rejected were then replaced via interpolation of the mean of the nearest neighboring channels (7.6 channels on average). Finally, we manually re-inspected the data to reject any trials containing residual noise. The final dataset included an average of 187 trials per subject (mean  $\pm$  SD [range] trials: 94  $\pm$  21 [55-119] lesioned visual hemifield, 93  $\pm$  22 [51-120] intact visual hemifield).

### Spatial Transformation

The surface Laplacian filter was applied to all clean EEG data to minimize volume conduction and maximize the accuracy of connectivity estimates [20–22]. Then, channels were swapped across the midline in patients with right-hemisphere lesions to normalize lesions to the left hemisphere [15–17]. The same swapping procedure was applied to 10 randomly chosen control datasets to preclude any inter-hemispheric variation from confounding lesion-related outcomes. Finally, the data were epoched into three segments per trial for analysis (see Figure 1B): (1) 500-ms pretrial baseline interval extending from 550–50 ms before the start screen; (2) 1,500-ms encoding-maintenance interval extending from the onset of the first stimulus; and (3) 900-ms active processing interval extending from the offset of the test prompt.

### Event-Related Potentials

The correct-trial 500-ms pretrial baseline, 1,500-ms encoding-maintenance, and 900-ms active processing EEG data segments were zero-padded to 7,500 to minimize filtering-induced edge artifacts and passed through a 30-Hz low-pass finite impulse response filter. Task-induced ERPs were computed over the encoding-maintenance and active processing intervals by absolute baseline-correcting the outputs on the temporal mean of the pretrial baseline.

## Spectral Decomposition

### Baseline Spectral Power

Power spectra were computed on all 500-ms pretrial baseline data segments. EEG data segments were zero-padded to 7,500 and multiplied with a Hanning taper. The fast Fourier transform was taken from the tapered signal and power was calculated from the complex Fourier output for each frequency between 1–40 Hz. For a similar approach, see [26].

### Time-Frequency Representations

Time-frequency representations of power were computed on the correct-trial 500-ms pretrial baseline, 1,500-ms encoding-maintenance, and 900-ms active processing data segments. EEG data segments were zero-padded to 7,500 ms and time-frequency representations were computed using an adaptive, frequency-dependent sliding time window of three cycles' length ( $\Delta t = 3/f$ ) for each frequency between 1–40 Hz [26]. The time windows were advanced in steps of 10 ms and the data in each window were multiplied with a Hanning taper before calculating power using fast Fourier transforms. As described below, statistical analysis of task-induced effects was performed over the encoding-maintenance and active processing intervals by standardizing the outputs on the pretrial baseline via bootstrapping [27].

### Phase Slope Index

To minimize contamination from simultaneous voltage changes on phase consistency, the trial-wise mean for correct-trial EEG data segments was subtracted from each correct-trial data segment (per visual hemifield for encoding-maintenance and active processing data segments) [22]. Time-frequency representations were computed from the outputs using the same parameters described above, with time windows advanced in steps of 100 ms. The Hanning taper confines the temporal spread to the specified taper length (here,  $\Delta t = 3/f$ ) and reduces spectral leakage, allowing us to keep the spectral bandwidth constant for computation of PSI. Cross-spectral density was calculated from the complex Fourier output for each frequency, from which time-resolved PSI was computed separately for the delta-theta (2–7 Hz) and alpha-beta (9–24 Hz) bands [29]. As described below, statistical analysis of task-induced effects was performed by first standardizing the outputs via bootstrapping [22], and then absolute baseline-correcting encoding-maintenance and active processing outputs on the temporal mean of the pretrial baseline.

### Graph Theory

The standardized pretrial baseline, encoding-maintenance, and active processing PSI outputs were assessed for network degrees – i.e., the weight of true directional connections between each channel and all other channels. This computation was performed on the standardized data so that true directional connections were defined as  $PSI |Z| > 1.96$  at an uncorrected  $\alpha$ -threshold of 0.05 (see description below). Task-induced directional networks were computed over the encoding-maintenance and active processing intervals by absolute baseline-correcting the outputs on the temporal mean of the pretrial baseline.

## QUANTIFICATION AND STATISTICAL ANALYSES

### Behavioral Analysis

Patient accuracy data ( $n = 14$  subjects) were submitted to a repeated-measures mixed ANCOVA with two visual hemifield (lesion, intact) and three condition (identity, spatial relation, temporal relation) within-subject factors, controlling for all between-subject factors (i.e., lesion hemisphere, etiology, and size, years elapsed since lesion incident, and patient age, gender, education, and IQ; see Table S1). No significant effects were observed, permitting the normalization of patient data into one group [24]. Results are presented in Table S2, and include  $F$  statistics, degrees of freedom (DF), partial  $\eta^2$  markers of effect size, and  $p$  values. The ANCOVA was performed in SPSS.

Accuracy was tested in a linear mixed-effects model with two group (patient, control), two visual hemifield, and three condition fixed effects, and 34 subject random effects [25]. The group main effect, and visual hemifield  $\times$  condition and three-way interaction effects passed an uncorrected  $\alpha$ -threshold of 0.05 (Table S3). However, results did not survive the Bonferroni correction for multiple comparisons (i.e., 3 main + 4 interaction effects [44]), which yielded an adjusted  $\alpha$ -threshold of  $0.05/7 \approx 0.0071$ . The same data were re-submitted to two models – one with group as the only fixed effect, and the other with only visual hemifield and condition fixed effects – to confirm that patients were significantly impaired at the task. Results of each model are presented in Table S3, and include  $F$  statistics, DF, Cohen's  $d$  markers of effect size for unequal groups, and  $p$  values. Accuracy data are presented in Figures 1C and 1D. Modeling was performed using the `fitglme.m` function in MATLAB.

### Statistical Bootstrapping

Bootstrapping analyses were performed using custom-built MATLAB code.

### Task-Induced Power

Task-induced power was analyzed per subject using a statistical bootstrapping procedure. Correct-trial time-frequency representations of power for the pretrial baseline were pooled into a single time-series for each channel and frequency, from which we randomly selected and averaged  $r$  data points ( $r =$  number of trials in that subject's dataset). This step was repeated 1,000 times to create normal distributions of channel/frequency-resolved pretrial baseline data. Encoding-maintenance and active processing raw power data were  $Z$  scored on the pretrial baseline distributions to assess the significance of task-induced effects. For a similar approach, see [27]. Results are presented in Figures 2 and S4, and include mean  $\pm$  SEM data by group.

### Phase Slope Index

Task-induced PSI was analyzed per subject using a statistical bootstrapping procedure followed by baseline correction. First, the frequency bins were randomly shuffled for each channel pair and time-frequency point, from which we re-computed PSI [29]. This step was repeated 1,000 times to create normal distributions of channel/time-frequency-resolved null PSI data. Pretrial baseline, encoding-maintenance, and active processing raw PSI data were Z scored on the null distributions to correct for any spurious results. For a similar approach, see [22]. True directional connections were defined as  $PSI |Z| > 1.96$  (i.e., uncorrected  $\alpha = 0.05$ ). Then, encoding-maintenance and active processing outputs were absolute baseline-corrected on the temporal mean of the pretrial baseline to isolate significant task-induced directionality (i.e., baseline-corrected  $\alpha = 0.05$ ). Results are presented in Figures 3 and 4, and include mean  $\pm$  SEM data by group and visual hemifield presentation.

### Cluster-Based Permutation Testing

Between-groups statistical testing of EEG data ( $n = 34$  subjects) employed a Monte Carlo method with cluster-based maximum correction for multiple comparisons [23]. An independent-samples  $t$  test was used to identify clusters of contiguous data points showing a difference between patients and controls, thresholded at 0.05, two-tailed, and then the  $t$  statistics were summed over all data points per cluster to calculate cluster size. Effects were clustered based on spatial adjacency, and on the time and/or frequency dimensions as appropriate. Then, group labels were randomly shuffled and the same clustering procedure was applied; this procedure was repeated 1000 times to create a normal distribution of null effects. Observed clusters were considered significant if fewer than 5% of randomizations yielded a larger effect (i.e., cluster-corrected  $\alpha = 0.05$ ). Statistical testing was performed using FieldTrip functions in MATLAB [36].

Baseline power was tested for main effects of group on all 64 channels. Task-induced ERP, power, and PSI data were tested separately for lesioned and intact visual hemifield presentations, and task-induced PSI network degree data were tested post hoc if significant group effects were detected in the PSI data. ERP results are presented in Figure S3, and include mean  $\pm$  SEM data by group and visual hemifield presentation, and significant  $t$  statistics masked on the BioSemi-64 topography. PSI results are presented in Figure 3, and include significant PSI and network degree effects masked on the BioSemi-64 topography. PSI results were visualized using the BrainNet Viewer for MATLAB [40].

Baseline power, and task-induced ERP and power data were also tested for group  $\times$  hemisphere interaction effects on all 54 non-midline channels. Hemisphere effects were modeled as indices of hemispheric asymmetry by subtracting the signal in each intact-hemisphere channel from its lesioned-hemisphere homolog (e.g.,  $F5 = F5 - F6$ ). In patients, values greater than zero indicate lesion  $>$  intact signals and values less than zero indicate lesion  $<$  intact signals. By calculating the equivalent indices in controls, we obtained reference data to submit to tests of group effects (i.e., group  $\times$  hemisphere interactions). ERP results are presented in the Results. Baseline power results are presented in Figure S3, and include mean  $\pm$  SEM data by group and significant  $t$  statistics masked on the BioSemi-64 topography. Task-induced power results are presented in Figure 2, and include mean  $\pm$  SEM data by group and visual hemifield presentation, and significant  $t$  statistics masked on the BioSemi-64 topography.

### DATA AND SOFTWARE AVAILABILITY

The data and custom-built MATLAB codes that support the current findings are deposited to the University of California, Berkeley, Collaborative Research in Computational Neuroscience database (<http://crcns.org>).